Electronic-structure calculations by first-principles density-based embedding of explicitly correlated systems

Niranjan Govind, Yan Alexander Wang, and Emily A. Carter[a)]
Department of Chemistry and Biochemistry, Box 951569, University of California, Los Angeles, California 90095-1569

(Received 19 October 1998; accepted 29 January 1999)

A first-principles embedding theory that combines the salient features of density functional theory (DFT) and traditional quantum chemical methods is presented. The method involves constructing a DFT-based embedding potential and then using it as a one-electron operator within a very accurate *ab initio* calculation. We demonstrate how DFT calculations can be systematically improved via this procedure. The scheme is tested using two closed shell systems, a toy model Li_2Mg_2, and the experimentally well characterized CO/Cu(111) system. Our results are in good agreement with near full configuration interaction calculations in the former case and experimental adsorbate binding energies in the latter. This method provides the means to systematically include electron correlation in a local region of a condensed phase. © *1999 American Institute of Physics.* [S0021-9606(99)31116-8]

I. INTRODUCTION

Atomic and molecular interactions with metal surfaces have been studied over the last 20 years using a number of well established theoretical techniques. These methods essentially fall into four major categories: finite cluster quantum chemistry, periodic slab density functional theory (DFT), embedded cluster methods, and Green's function DFT of semi-infinite crystals.

Traditional quantum chemistry methods have been used to study the energetics of adsorbate-surface interactions for a number of years. These methods, though formally correct, can only be applied to study small fragments of representative surfaces and clusters[1] due to their highly nonlinear scaling properties. As a result, important long-range contributions from the surrounding surface and bulk atoms are neglected, compromising the overall accuracy of the predicted energetics. Modifications of the finite cluster model to account for the background Fermi sea of electrons and to compensate for the lack of a proper band structure have been developed by Nakatsuji and Rösch, respectively. Nakatsuji's dipped adcluster model (DAM),[2] for example, uses a chemical potential (e.g., the work function of the metal) to optimize the charge on a small cluster. It also takes into account an image charge correction. This is a purely classical electrostatic approach and accounts for the background electrons in an implicit manner. The scheme proposed by Rösch[3] introduces a Gaussian broadening of the cluster energy levels to emulate a metallic band structure. In any case, *ab initio* quantum chemical methods cannot be used on very large clusters or extended systems, as they quickly become unwieldy for reasons already mentioned.

On the other hand, periodic slab DFT calculations[4–9] are relatively inexpensive and quite capable of dealing with infinite systems such as bulk solids, solid surfaces and interfaces, but this comes at a price. These calculations are limited by the approximate density functional representations [local-density approximation (LDA)[10,11]/generalized gradient approximation (GGA)[12–15]] for the electron exchange and correlation.[16] These are accurate for predicting structures but can overestimate adsorbate-surface binding energies by up to ~ 1 eV, for example, with the LDA.[11] A number of studies have shown that the GGAs do not always systematically improve LDA results.[17] Nonetheless, development of nonlocal corrections to the LDA remains an active area of research.[18]

The embedded cluster method[19,20,22–33] is a technique that straddles the cluster and slab models. The attractive feature of the embedded cluster idea is that it preserves the strengths of the cluster approach, namely, it allows one to describe the very local chemisorption process to a high degree of accuracy in the presence of a surrounding lattice. This approach has been implemented in a number of different forms where a designated cluster is embedded in an array of point charges,[24,25] shell model background[26] or in a dielectric medium.[27,28] These models have been used quite successfully in dealing with ionic and covalent condensed phases. However, in metallic systems, the scenario is very different and warrants a more precise treatment of the embedding potential. The scheme proposed by Ellis *et al.*[19] was one of the earliest in this spirit. Their method consists of a cluster embedded in a crystal charge density constructed by superposition of periodic images of the cluster charge density, iterated to self-consistency within a DFT cluster-in-DFT slab/bulk model. The Kohn-Sham (KS) equations for the cluster orbitals are solved in the presence of this density, but because there are no orbitals in the surroundings, there is no way to orthogonalize the cluster orbitals to the orbitals of environment. This is fixed up in the Ellis embedding scheme by tailored repulsive potentials that force the electrons in the cluster to stay out of the cores of the surrounding atoms, introducing a degree of empiricism into the method. An al-

a)Electronic mail: eac@chem.ucla.edu

ternate way around this problem was proposed and applied within a DFT-in-DFT embedding scheme by Cortona,[20] where kinetic-energy cross terms are explicitly included. This method has since been applied in a similar fashion by Wesolowski, Warshal, and Weber [22] to examine a solute in solution and by Truong and co-workers to study the adsorption of water on NaCl(001).[23] Our method, discussed in subsequent sections, is related to these ideas.

In the early 80's, Whitten *et al.*[29] developed the first cluster-in-cluster embedding scheme. In essence, their method consisted of: solving for a self-consistent field (SCF) minimum basis set (one 4*s* orbital/atom) description of a large cluster (e.g., ~30–100 atoms), localizing the orbitals via exchange energy maximization, using these localized orbitals to set up the effective Coulomb and exchange operators for the electrons associated with the embedded cluster and performing a relatively small configuration interaction (CI) calculation within the orbitals localized on the embedded cluster. This strategy provides an approximate way of accounting for nearby electrons outside the embedded cluster itself. The theory enables the treatment of localized chemisorption processes using correlated wave functions, but is limited to a cluster description of the background. The main drawback of cluster-in-cluster methods is that the embedding operators are derived from a wave function that does not describe a metal properly: one needs a two-dimensionally infinite wave function/density with the proper band structure. In fact, a recent discussion[34] has appeared pointing out a number of problems with such cluster-in-cluster models. These include the lack of marked improvement of the results over finite clusters of the same size, problems with the orbital space partitioning such that charge conservation is violated, spurious mixing of virtual orbitals into the density matrix, the inherent delocalized nature of metallic orbitals, etc. Nevertheless, this model has proved quite successful in describing a variety of chemisorption situations. Modified versions of the scheme have also been applied to an extended background,[30] within a DFT framework,[31,32] and in conjunction with second-order perturbation theory.[33]

The perturbed cluster technique of Pisani[37] and extensions[38] as well as the closely related Green's function formulations[39–42] provide a different embedding paradigm. The Green's function method, for example, yields a proper description of the bare metal's bulk and surface states and can be utilized to study local chemisorption and bulk defects very effectively, but the exchange and correlation are treated in exactly the same way as in periodic slab DFT calculations. It is not obvious how this formalism could be generalized to explicit correlation methods[43] like multiconfiguration SCF (MCSCF), Møller-Plesset perturbation theory (MPn), coupled cluster and CI calculations. The local space approximation of Kirtman and co-workers should also be mentioned in the context of embedding. This approach again deconstructs the problem into an unperturbed density matrix and a correction due to the adsorbate, which can be treated with explicit correlation methods.[44]

In this article, we present a new scheme that combines conventional *ab initio* and DFT methods. An effort in this direction has been reported recently by Abarenkov *et al.*,[45]

FIG. 1. Partitioning of the system. The figure on the left represents a local chemisorption situation, whereas the figure on the right represents a localized defect embedded in a bulk phase. The shading scheme shown is maintained in all subsequent figures.

where a MCSCF cluster was embedded in a LDA cluster background. Our model treats the extended parts of the system in a periodic DFT-LDA/GGA fashion and the local region of interest as an embedded cluster described via explicit correlation methods. The scheme is well suited to deal with adsorption at low coverages as well as local defects or solutes embedded in a condensed phase. The embedding scheme presented here seeks an accurate description of a local region of interest yet also requires a full calculation on the extended background via DFT. This is in contrast to most previous embedding strategies that utilize an unperturbed treatment of the background in order to construct a nonself-consistent embedding potential. These previous approaches had as a goal to reduce the expense of treating a large system; our goal is accuracy, not reduction of expense at this point.

The paper is organized as follows. We develop the theoretical framework and discuss the implications of the scheme in Sec. II. Practical implementation details are provided in Sec. III. Applications of the method appear in Sec. IV. We offer perspective and conclusions in Sec. V.

II. THEORETICAL MODEL

A. Formulation

Embedding theories are generally based on a systematic partitioning of the total system. This is also the starting point for our method. From here on, the cluster portion or the region of interest of the system will be referred to as Region I and the background as Region II (Fig. 1).

With this partitioning, one can formally write down the total energy as

$$E_{\mathrm{tot}} = E_{\mathrm{I}} + E_{\mathrm{II}} + E_{\mathrm{int}}, \tag{1}$$

which can further be expressed in detail as

$$E_{\mathrm{tot}} = \langle \Psi_{\mathrm{tot}} | \hat{H}_{\mathrm{I}} + \hat{H}_{\mathrm{II}} + \hat{H}_{\mathrm{int}} | \Psi_{\mathrm{tot}} \rangle \tag{2}$$

in terms of the subsystem and interaction Hamiltonians $\hat{H}_{\mathrm{I}}$, $\hat{H}_{\mathrm{II}}$, $\hat{H}_{\mathrm{int}}$ and the total normalized many-body wave function Ψ_{tot}. Things can be made further transparent if one views the problem from a DFT standpoint, which is formally exact, and rewrites Eq. (1) as[46]

$$E_i = T_s[\rho_i] + E^i_{\mathrm{ne}}[\rho_i] + E_{\mathrm{xc}}[\rho_i] + J[\rho_i] + E^i_{\mathrm{nn}} \tag{3}$$

with $i=\mathrm{I}, \mathrm{II}, \mathrm{tot}$. Here, T_s, E_{ne}, J, E_{xc} and E_{nn} are the non-interacting kinetic, electron-nuclear attraction, Hartree repulsion, exchange-correlation and nuclear-nuclear repulsion energy functionals, respectively. The interaction energy can be written in a similar manner as

$$E_{\mathrm{int}}=T_s^{\mathrm{int}}+E_{\mathrm{ne}}^{\mathrm{int}}+E_{\mathrm{xc}}^{\mathrm{int}}+J^{\mathrm{int}}+E_{\mathrm{nn}}^{\mathrm{int}}, \tag{4}$$

where the individual terms on the right side of the above equation are given by

$$T_s^{\mathrm{int}}=T_s[\rho_{\mathrm{tot}}]-T_s[\rho_{\mathrm{I}}]-T_s[\rho_{\mathrm{II}}], \tag{5}$$

$$\begin{aligned}E_{\mathrm{ne}}^{\mathrm{int}}&=E_{\mathrm{ne}}^{\mathrm{tot}}[\rho_{\mathrm{tot}}]-E_{\mathrm{ne}}^{\mathrm{I}}[\rho_{\mathrm{I}}]-E_{\mathrm{ne}}^{\mathrm{II}}[\rho_{\mathrm{II}}]\\&=\langle v_{\mathrm{ne}}^{\mathrm{I}}(\mathbf{r})|\rho_{\mathrm{II}}(\mathbf{r})\rangle+\langle v_{\mathrm{ne}}^{\mathrm{II}}(\mathbf{r})|\rho_{\mathrm{I}}(\mathbf{r})\rangle,\end{aligned} \tag{6}$$

$$E_{\mathrm{xc}}^{\mathrm{int}}=E_{\mathrm{xc}}[\rho_{\mathrm{tot}}]-E_{\mathrm{xc}}[\rho_{\mathrm{I}}]-E_{\mathrm{xc}}[\rho_{\mathrm{II}}], \tag{7}$$

$$J^{\mathrm{int}}=J[\rho_{\mathrm{tot}}]-J[\rho_{\mathrm{I}}]-J[\rho_{\mathrm{II}}]=\left\langle \rho_{\mathrm{I}}(\mathbf{r})\left|\frac{1}{|\mathbf{r}-\mathbf{r}'|}\right|\rho_{\mathrm{II}}(\mathbf{r}')\right\rangle, \tag{8}$$

$$E_{\mathrm{nn}}^{\mathrm{int}}=E_{\mathrm{nn}}^{\mathrm{tot}}-E_{\mathrm{nn}}^{\mathrm{I}}-E_{\mathrm{nn}}^{\mathrm{II}} \tag{9}$$

with $\rho_{\mathrm{tot}}(\mathbf{r})=\rho_{\mathrm{I}}(\mathbf{r})+\rho_{\mathrm{II}}(\mathbf{r})$. Given these definitions, one can construct Region I's embedding potential $v_{\mathrm{emb}}(\mathbf{r})$ due to Region II by performing a functional derivative with respect to $\rho_{\mathrm{I}}(\mathbf{r})$, with the assumption that $\rho_{\mathrm{I}}(\mathbf{r})$ and $\rho_{\mathrm{II}}(\mathbf{r})$ are independent functions,

$$v_{\mathrm{emb}}(\mathbf{r})=\frac{\delta E_{\mathrm{int}}}{\delta\rho_{\mathrm{I}}(\mathbf{r})}=\frac{\delta T_s^{\mathrm{int}}}{\delta\rho_{\mathrm{I}}(\mathbf{r})}+\frac{\delta E_{\mathrm{ne}}^{\mathrm{int}}}{\delta\rho_{\mathrm{I}}(\mathbf{r})}+\frac{\delta E_{\mathrm{xc}}^{\mathrm{int}}}{\delta\rho_{\mathrm{I}}(\mathbf{r})}+\frac{\delta J^{\mathrm{int}}}{\delta\rho_{\mathrm{I}}(\mathbf{r})}, \tag{10}$$

with

$$\begin{aligned}\frac{\delta T_s^{\mathrm{int}}}{\delta\rho_{\mathrm{I}}(\mathbf{r})}&=\frac{\delta T_s[\rho_{\mathrm{tot}}]}{\delta\rho_{\mathrm{tot}}(\mathbf{r})}\frac{\delta\rho_{\mathrm{tot}}(\mathbf{r})}{\delta\rho_{\mathrm{I}}(\mathbf{r})}-\frac{\delta T_s[\rho_{\mathrm{I}}]}{\delta\rho_{\mathrm{I}}(\mathbf{r})}\\&=\frac{\delta T_s[\rho_{\mathrm{tot}}]}{\delta\rho_{\mathrm{tot}}(\mathbf{r})}-\frac{\delta T_s[\rho_{\mathrm{I}}]}{\delta\rho_{\mathrm{I}}(\mathbf{r})},\end{aligned} \tag{11}$$

$$\frac{\delta E_{\mathrm{ne}}^{\mathrm{int}}}{\delta\rho_{\mathrm{I}}(\mathbf{r})}=v_{\mathrm{ne}}^{\mathrm{II}}(\mathbf{r}), \tag{12}$$

$$\begin{aligned}\frac{\delta E_{\mathrm{xc}}^{\mathrm{int}}}{\delta\rho_{\mathrm{I}}(\mathbf{r})}&=\frac{\delta E_{\mathrm{xc}}[\rho_{\mathrm{tot}}]}{\delta\rho_{\mathrm{tot}}(\mathbf{r})}\frac{\delta\rho_{\mathrm{tot}}(\mathbf{r})}{\delta\rho_{\mathrm{I}}(\mathbf{r})}-\frac{\delta E_{\mathrm{xc}}[\rho_{\mathrm{I}}]}{\delta\rho_{\mathrm{I}}(\mathbf{r})}\\&=\frac{\delta E_{\mathrm{xc}}[\rho_{\mathrm{tot}}]}{\delta\rho_{\mathrm{tot}}(\mathbf{r})}-\frac{\delta E_{\mathrm{xc}}[\rho_{\mathrm{I}}]}{\delta\rho_{\mathrm{I}}(\mathbf{r})},\end{aligned} \tag{13}$$

$$\frac{\delta J^{\mathrm{int}}}{\delta\rho_{\mathrm{I}}(\mathbf{r})}=\int\frac{\rho_{\mathrm{II}}(\mathbf{r}')}{|\mathbf{r}-\mathbf{r}'|}d\tau'=\int\frac{\rho_{\mathrm{tot}}(\mathbf{r}')-\rho_{\mathrm{I}}(\mathbf{r}')}{|\mathbf{r}-\mathbf{r}'|}d\tau'. \tag{14}$$

Similar equations have been derived by Cortona in the context of a pure DFT-in-DFT embedding scheme;[20] a difference here is that while terms involving ρ_{tot} will be calculated once and for all from a DFT calculation, the terms involving ρ_{I} will be updated self-consistently from a molecular quantum chemistry calculation.

B. Embedding implications

The role of the embedding thus described can be revealed succinctly by rewriting Eq. (1) as

$$E_{\mathrm{tot}}\approx E_{\mathrm{tot}}^{\mathrm{emb}}=E_{\mathrm{I}}^{\mathrm{ab}}+E_{\mathrm{II}}^{\mathrm{DFT}}+E_{\mathrm{int}}^{\mathrm{DFT}}, \tag{15}$$

where $E_{\mathrm{I}}^{\mathrm{ab}}$ is the *ab initio* energy of Region I in the presence of $v_{\mathrm{emb}}(\mathbf{r})$, $E_{\mathrm{II}}^{\mathrm{DFT}}$ is the DFT energy of Region II, and $E_{\mathrm{int}}^{\mathrm{DFT}}$ is the DFT interaction energy. Adding and subtracting $E_{\mathrm{I}}^{\mathrm{DFT}}$ [the DFT energy of Region I in the presence of $v_{\mathrm{emb}}(\mathbf{r})$] to the right side of the above equation and rearranging, we get

$$\begin{aligned}E_{\mathrm{tot}}^{\mathrm{emb}}&=E_{\mathrm{I}}^{\mathrm{DFT}}+E_{\mathrm{II}}^{\mathrm{DFT}}+E_{\mathrm{int}}^{\mathrm{DFT}}+(E_{\mathrm{I}}^{\mathrm{ab}}-E_{\mathrm{I}}^{\mathrm{DFT}})\\&=E_{\mathrm{tot}}^{\mathrm{DFT}}+(E_{\mathrm{I}}^{\mathrm{ab}}-E_{\mathrm{I}}^{\mathrm{DFT}}).\end{aligned} \tag{16}$$

Clearly, the difference between $E_{\mathrm{I}}^{\mathrm{ab}}$ and $E_{\mathrm{I}}^{\mathrm{DFT}}$ corrects $E_{\mathrm{tot}}^{\mathrm{DFT}}$. Also notice that $E_{\mathrm{II}}^{\mathrm{DFT}}$ does not appear explicitly as it has already been accounted for in the evaluation of $E_{\mathrm{tot}}^{\mathrm{DFT}}$. Equation (16) resembles the IMOMM/IMOMO family of methods[21] where the energy of the total system is first evaluated at a lower level of theory and corrections are added by calculating energy differences of the region of interest at low and high levels of theory. Our method is formally distinct from Morukuma's approach in that the region of interest (Region I) is not treated in isolation but rather is treated in the presence of an embedding potential.

C. Variational domain

Of the functions $\rho_{\mathrm{I}}(\mathbf{r})$, $\rho_{\mathrm{II}}(\mathbf{r})$, and $\rho_{\mathrm{tot}}(\mathbf{r})$, only two of them are independent. One can choose $\rho_{\mathrm{I}}(\mathbf{r})$ and $\rho_{\mathrm{tot}}(\mathbf{r})$ as the independent variables. In principle, one should really think of the two-stage minimization process in the spirit of the Levy constrained search[46,47]

$$\min_{\rho_{\mathrm{tot}}}\min_{\rho_{\mathrm{I}}}E_{\mathrm{tot}}^{\mathrm{emb}}[\rho_{\mathrm{tot}},\rho_{\mathrm{I}}]. \tag{17}$$

However, experience[46] has shown that $\rho_{\mathrm{tot}}(\mathbf{r})$ obtained via DFT is a good representation of the true total density. We therefore keep it fixed, and simplify the above equation

$$\min_{\rho_{\mathrm{I}}}E_{\mathrm{tot}}^{\mathrm{emb}}[\rho_{\mathrm{tot}},\rho_{\mathrm{I}}], \tag{18}$$

with the variation domain

$$\{\rho_{\mathrm{I}}(\mathbf{r}),\rho_{\mathrm{II}}(\mathbf{r})|\rho_{\mathrm{I}}(\mathbf{r})+\rho_{\mathrm{II}}(\mathbf{r})\equiv\rho_{\mathrm{tot}}(\mathbf{r})\}. \tag{19}$$

Therefore, all terms involving $\rho_{\mathrm{tot}}(\mathbf{r})$ are evaluated with fixed $\rho_{\mathrm{tot}}(\mathbf{r})$. This greatly accelerates the search for the variational minimum of $E_{\mathrm{tot}}^{\mathrm{emb}}$.

III. IMPLEMENTATION

A. Computational procedure

There are a number of issues to deal with in the practical realization of the theory. These steps constitute the main aspects of the implementation:

Step 1: A well converged $\rho_{\mathrm{tot}}(\mathbf{r})$ is first calculated by solving the single-particle KS[48] equations for the whole system

$$(-\tfrac{1}{2}\nabla^2+V_{\mathrm{eff}}^{\mathrm{KS}}(\mathbf{r}))\psi_{\mathrm{tot}}^i(\mathbf{r})=\epsilon_{\mathrm{KS}}^i\psi_{\mathrm{tot}}^i(\mathbf{r}), \tag{20}$$

where the KS effective potential $V_{\mathrm{eff}}^{\mathrm{KS}}(\mathbf{r})$ is given by

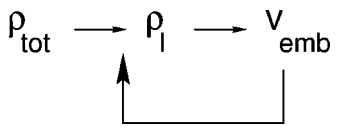

FIG. 2. Schematic diagram of the embedding procedure.

$$V_{\rm eff}^{\rm KS}(\mathbf{r}) = v_{\rm ne}^{\rm tot}(\mathbf{r}) + \frac{\delta E_{\rm xc}[\rho_{\rm tot}]}{\delta \rho_{\rm tot}(\mathbf{r})} + \frac{\delta J[\rho_{\rm tot}]}{\delta \rho_{\rm tot}(\mathbf{r})}, \tag{21}$$

the density by

$$\rho_{\rm tot}(\mathbf{r}) = \sum_i n^i |\psi_{\rm tot}^i(\mathbf{r})|^2, \tag{22}$$

and $\{n^i\}$, $\{\epsilon_{\rm KS}^i\}$, and $\{\psi_{\rm tot}^i\}$ are the occupation numbers, KS eigenvalues, and KS orbitals, respectively.

Step 2: A reasonable first guess for $\rho_{\rm I}(\mathbf{r})$ is constructed for the atoms in Region I either by solving the SCF equations for the cluster atoms without $v_{\rm emb}(\mathbf{r})$ or by a superposition of atomic densities. For the Hartree-Fock (HF) method,[43] we solve

$$\sum_\nu F_{\mu\nu} C_{\nu,i} = \epsilon_{\rm HF}^i \sum_\nu S_{\mu\nu} C_{\nu,i}, \tag{23}$$

where the orbitals are expanded in terms of basis functions $\{\phi_\nu\}$

$$\psi_i^{\rm HF}(\mathbf{r}) = \sum_\nu C_{\nu,i} \phi_\nu(\mathbf{r}), \tag{24}$$

and the density is given by

$$\rho_{\rm I}^{\rm HF}(\mathbf{r}) = \sum_i^{\rm occ} \sum_{\mu,\nu} C_{\mu,i}^* C_{\nu,i} \phi_\mu^*(\mathbf{r}) \phi_\nu(\mathbf{r}), \tag{25}$$

where $C_{\nu,i}$ are the HF molecular orbital expansion coefficients, and $F_{\mu\nu}$ and $S_{\mu\nu}$ are the Fock and overlap matrices, respectively; i runs over all the occupied orbitals in the cluster. Similar equations can be derived for other self-consistent *ab initio* procedures.[43]

Step 3: $v_{\rm emb}(\mathbf{r})$ is then constructed according to Eqs. (10)–(14) using $\rho_{\rm tot}(\mathbf{r})$ and $\rho_{\rm I}(\mathbf{r})$.

Step 4: The effective one-electron operator $v_{\rm emb}(\mathbf{r})$ is then expressed in matrix form in the cluster basis, inserted into the SCF equations, and $\rho_{\rm I}(\mathbf{r})$ is updated.

$$\sum_\nu (F_{\mu\nu} + M_{\mu\nu}) C_{\nu,i} = \gamma_{\rm HF}^i \sum_\nu S_{\mu\nu} C_{\nu,i}, \tag{26}$$

$$M_{\mu\nu} = \langle \phi_\mu(\mathbf{r}) | v_{\rm emb}(\mathbf{r}) | \phi_\nu(\mathbf{r}) \rangle, \tag{27}$$

where $\{\gamma_{\rm HF}^i\}$ are the new orbital energies.

Step 5: Steps 3 and 4 are performed repeatedly until full self-consistency is achieved (Fig. 2). It must be noted that $\rho_{\rm tot}(\mathbf{r})$ is kept fixed during the entire process in accordance with the definition of the variational domain described earlier in Eq. (19). Post-SCF perturbative corrections (MPn) are then calculated using the converged $\rho_{\rm I}(\mathbf{r})$.

We emphasize that Eq. (27) is completely general regardless of the representation. In our implementation we evaluate the various contributions to $v_{\rm emb}$ as follows: the long-range terms (the local part of the pseudopotential and Hartree potential) are easily treated in reciprocal space using fast Fourier transforms. This implicitly relies on a uniform real space grid. The short-range exchange-correlation contribution is also calculated on the same uniform real space grid, while the short-range, nonlocal pseudopotential contribution was evaluated analytically in real space. Since $M_{\mu\nu}$ requires a ''sandwich'' of the potential between the basis functions, the grid-based terms (kinetic, Hartree and the local part of pseudopotential) can become expensive to construct (depending on the fineness of the grid and the number of basis functions in the calculation) as one needs to evaluate the potential on the entire grid. Details concerning the construction of $v_{\rm emb}(\mathbf{r})$ are presented in Sec. III C.

With regard to neutrality and particle number in the two regions, Region I is kept neutral and the number of electrons in Region I is kept fixed because HF and MPn theories can only be applied to integer particle numbers.[43] However, since $v_{\rm emb}(\mathbf{r})$ is constantly updated via all the terms that depend on $\rho_{\rm tot}(\mathbf{r})$ and $\rho_{\rm I}(\mathbf{r})$, $\rho_{\rm I}(\mathbf{r})$ is allowed to evolve to self-consistency without any rigid spatial confinement, which effectively allows charge density changes in both regions.

B. Programs and densities

The method was implemented using suitably modified versions of the plane-wave-based DFT program CASTEP[49] and the Gaussian-function-based *ab initio* program HONDO.[50] Converged $\rho_{\rm tot}(\mathbf{r})$ were obtained using well documented plane-wave DFT techniques naturally suited for periodic systems.[49,51] Standard norm-conserving pseudopotentials[52] were used for the respective atoms and the LDA[10] or the GGA[14] for the exchange and correlation. Calculations on the cluster SCF part were performed using HONDO. To enable simultaneous manipulation of $\rho_{\rm I}(\mathbf{r})$ and $\rho_{\rm tot}(\mathbf{r})$ in the evaluation of $v_{\rm emb}(\mathbf{r})$, both densities were represented[53] on the same Cartesian grid.

C. Embedding potential

We now discuss implementation of the individual terms of the embedding potential.

1. Kinetic-energy contribution - $\delta T_s^{\rm int}/\delta\rho$

The kinetic-energy contribution to $v_{\rm emb}(\mathbf{r})$ is the most challenging component. Since the exact analytic form of the kinetic-energy density functional (KEDF) $T_s[\rho]$ is not known, it is not clear how to construct a kinetic-energy potential exactly. One therefore needs to use approximate forms $T_s^{\rm approx}[\rho]$ instead. Although many approximate KEDFs have been developed over the years, they lack transferability, i.e., they cannot be applied with the same merits in different environments.[46] In addition, there is the subtle but important question of the accuracy of the KEDF and its potential. We first present a discussion of different KEDFs and their properties before presenting applications.

The conventional gradient expansion is the oldest strategy, where the KEDF is approximated by a gradient expansion around a slowly varying electron density, normally written as[46]

$$T_s^{\text{approx}}[\rho] \approx \langle t_0(\rho) + t_2(\rho, \nabla\rho) + t_4(\rho, \nabla\rho, \nabla^2\rho) + t_6(\rho, \nabla\rho, \nabla^2\rho, \nabla^3\rho) + \cdots \rangle. \quad (28)$$

The zeroth-order term t_0 yields the Thomas-Fermi (TF) functional[54] and is purely a function of $\rho(\mathbf{r})$. The second-order term t_2 is one-ninth of the original von Weizsäcker (vW) correction[55] and is a function of $\rho(\mathbf{r})$ and $\nabla\rho(\mathbf{r})$. It is fairly easy to show that the TF functional is exact only at the free-electron limit or $\mathbf{G}\rightarrow 0$ in reciprocal space, and that the vW functional is exact for one- and two-electron ground state systems but fails for a many-electron environment.[46] The gradient expansion does improve the TF term, but diverges beyond fourth order for exponentially decaying densities and produces algebraically decaying densities and no shell structure for atoms.[46] In fact, t_4 has a divergent functional derivative and t_6 diverges for atoms and molecules.[46] Extensions of this model have been used, where the strength of the vW term is controlled by a parameter λ, i.e., $\lambda = \frac{1}{5}$.[46,56,57]

The Lee-Lee-Parr approach[58] based on a conjointness assumption between KEDFs and exchange functionals is another scheme used to construct KEDFs. These functionals typically take the form

$$T_s^{\text{approx}}[\rho] \approx \langle t_0(\rho) | f(\rho, \nabla\rho) \rangle. \quad (29)$$

The function $f(\rho, \nabla\rho)$ in the above equation is an enhancement factor that depends on $\rho(\mathbf{r})$ and $\nabla\rho(\mathbf{r})$ and is identical to the enhancement factor of the corresponding exchange functional. One can obtain many different KEDFs starting from different exchange functionals in this manner.

The approximate KEDF models discussed thus far fall short of reproducing one important property. They do not have the right linear-response (LR) behavior[59] which is required to produce the correct screening potential and the consequent Friedel oscillations. The Friedel oscillations arise as a result of the discontinuity at the Fermi surface and a weak logarithmic singularity at $\mathbf{G} = 2k_F$ in the exact susceptibility, given by the Lindhard LR function for a noninteracting electron gas without exchange[60,61] (Fig. 3). The exact screening potential as a result has a slowly decaying oscillatory part

$$v_{\text{scr}}^{\text{exact}}(\mathbf{r}) \approx \frac{\cos(2k_F r)}{r^3}, \quad (30)$$

where the Fermi momentum $k_F = (3\pi^2\rho_0)^{1/3}$ and ρ_0 is the average electron density. The TF functional, for instance, yields an incorrect Yukawa-like screening potential that results from an incorrect constant susceptibility in reciprocal space, leading to no Friedel oscillations. The vW term, on the other hand, corrects the TF susceptibility but is still inadequate. Approximate KEDFs with exact LR in principle can be constructed in the following manner:[62–65]

$$T_s^{\alpha}[\rho] = T_{\text{TF}}[\rho] + T_{\text{vW}}[\rho] + T_X^{\alpha}[\rho], \quad (31)$$

$$T_{\text{TF}}[\rho] = \frac{3(3\pi^2)^{2/3}}{10} \left\langle \rho(\mathbf{r})^{5/3} \right\rangle, \quad (32)$$

$$T_{\text{vW}}[\rho] = \frac{1}{8} \left\langle \frac{|\nabla\rho(\mathbf{r})|^2}{\rho(\mathbf{r})} \right\rangle, \quad (33)$$

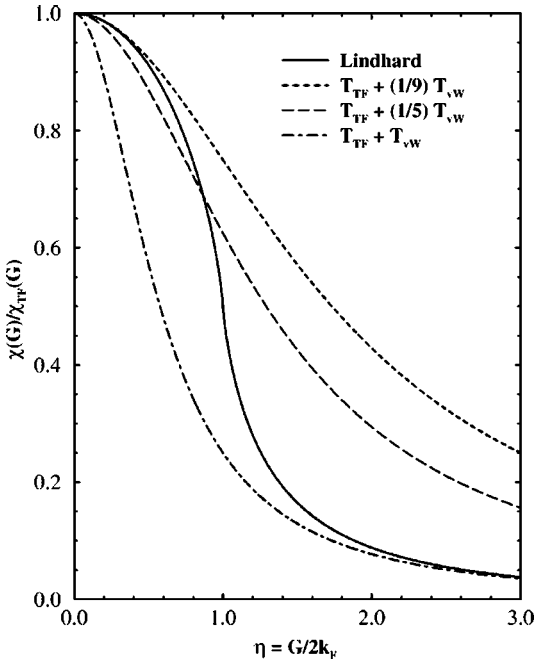

FIG. 3. Linear response behavior of various functionals in reciprocal space. All the functionals are normalized to the Thomas-Fermi response $\chi_{\text{TF}} = -(k_F/\pi^2)$.

$$T_X^{\alpha}[\rho] = \langle \rho(\mathbf{r})^{\alpha} | K_{\alpha}(\mathbf{r} - \mathbf{r}') | \rho(\mathbf{r}')^{\alpha} \rangle, \quad (34)$$

where α is some positive number. The kernel $K_{\alpha}(\mathbf{r} - \mathbf{r}')$ is chosen so that T_s^{α} satisfies the exact Lindhard LR. In Fourier space, this is given by

$$\hat{F}\left(\frac{\delta^2 T_s^{\alpha}[\rho]}{\delta\rho(\mathbf{r})\,\delta\rho(\mathbf{r}')}\bigg|_{\rho_0} \right) = -\frac{1}{\chi_{\text{Lind}}} = \frac{\pi^2}{k_f}\left(\frac{1}{2} + \frac{1-\eta^2}{4\eta} \ln\left| \frac{1+\eta}{1-\eta} \right| \right)^{-1}, \quad (35)$$

where $\eta = G/(2k_F)$ is a dimensionless momentum and χ_{Lind} is the Lindhard susceptibility function in reciprocal space.[60,61] $K_{\alpha}(\mathbf{r} - \mathbf{r}')$ can then be expressed in reciprocal space as

$$\hat{F}K_{\alpha}(\mathbf{r} - \mathbf{r}') = \tilde{K}_{\alpha}(\mathbf{G}) = -\frac{\chi_{\text{Lind}}^{-1} - \chi_{\text{vW}}^{-1} - \chi_{\text{TF}}^{-1}}{2\alpha^2 V \rho_0^{2(\alpha-1)}}, \quad (36)$$

where V is the simulation cell volume, and $\chi_{\text{TF}} = -(k_F/\pi^2)$ and $\chi_{\text{vW}} = \chi_{\text{TF}}/(3\eta^2)$ are the TF and vW LR functions, respectively.

The LR corrections can also be rigorously derived from a perturbation picture by expanding around ρ_0.[66] Higher-order corrections can also be worked out in a similar manner.[62,67] These KEDFs have been successfully used to study the bulk phases of free-electron-like elements like Na[64] and nearly free-electron elements like Al,[64,65] where density variations are moderate. It has also been used to study the diamond structure of Si.[62]

Despite the success of these functionals with bulk materials, they are unsuitable in situations where there are large density variations like atoms, molecules, and surfaces. This stems from the dependence of the above formulas on ρ_0 and

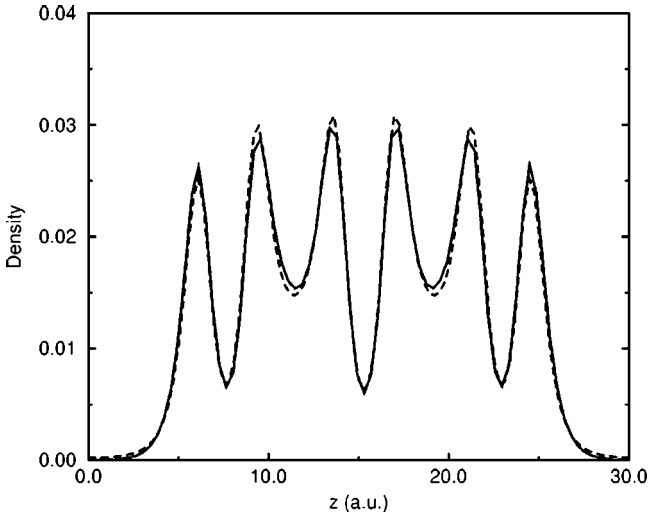

FIG. 4. Surface density profile of a five-layer Al(100) slab. The solid line represents the KS density and the dotted line, the self-consistent density using Eq. (31) with $\alpha=\frac{5}{6}$.

k_F. It is conceivable that one can generalize Eq. (31) by defining a local $k_F(\mathbf{r})=(3\pi^2\rho(\mathbf{r}))^{1/3}$ or an averaged local k_F as is commonly done in exchange-correlation functionals. This, however, would be inconsistent with the derivation of the response kernel $K_\alpha(\mathbf{r}-\mathbf{r}')$ which is intrinsically based on an expansion around ρ_0 and consequently a constant k_F.

In fact a ''blind'' application[59] of Eqs. (31)–(36) in a self-consistent density-based Hohenberg-Kohn (SCDBHK) scheme,[68] for example, to Al surfaces yields surface energies 2–3 times larger than corresponding KS values, even though the surface electron density profiles agree very well[59] (see Fig. 4). This implies that a good potential does not necessarily imply a good KEDF. Other approximate KEDFs do exist that can yield accurate energies when good densities are inserted,[46,59,69] but these can differ greatly if evaluated via the SCDBHK scheme with their corresponding potentials. One can also name several other examples[59] of ''good energy'' KEDFs with ill-behaved potentials. In short, it is not only important to choose a good functional in terms of the energy but also in terms of the potential, and vice versa.

Functionals discussed so far fall into a class where the kernels are density independent, i.e., $K(\mathbf{r}-\mathbf{r}')$. Over the last few years there have been a number of efforts to generalize them to include a density dependence, i.e., $K(\rho(\mathbf{r}),\rho(\mathbf{r}'),\mathbf{r}-\mathbf{r}'))$,[59,70] by taking into account all the important limits. Although these functionals do reproduce the atomic shell structure and yield surface energies that are in good agreement with KS jellium calculations, realistic applications appear numerically prohibitive (scaling quadratically with grid size) due to the nature of their makeup.

As seen from the above discussion, the KEDF must be chosen with care. Judging by the results of Fig. 4, it appears that we are able to obtain good KEDF potentials (that yield a good density) while the ''goodness'' of the KEDF energies remains to be demonstrated. We shall give details of the T_s functionals chosen for the embedding study, how they were evaluated, and the quality of the results in the applications section.

2. Ion-electron contribution $-\delta E_{ne}^{int}/\delta\rho_I$

The ionic interaction $v^{II}(\mathbf{r})$ was represented by conventional norm-conserving pseudopotentials[52] where the potential was decomposed into a long-range local part and a short-range, angular-momentum-dependent, nonlocal part

$$\hat{v}^{II}(\mathbf{r})=\sum_j\sum_{l=0}^{\infty}\sum_{m=-l}^{l}\hat{v}_l(\mathbf{r}-\mathbf{R}_j)|lm\rangle\langle lm|$$
$$=\sum_j\hat{v}_{loc}(\mathbf{r}-\mathbf{R}_j)+\sum_j\sum_{l=0}^{l_{max}-1}\sum_{m=-l}^{l}|lm\rangle(\hat{v}_l(\mathbf{r}-\mathbf{R}_j)$$
$$-\hat{v}_{loc}(\mathbf{r}-\mathbf{R}_j))\langle lm|=v_{loc}(\mathbf{r})+v_{nonloc}(\mathbf{r}), \quad (37)$$

where j runs over the embedding ions, $|lm\rangle\langle lm|$ are spherical harmonic projection operators, l is the angular momentum of the relevant channel and l_{max} is typically one greater than the highest angular component of any core orbital. The local part $v_{loc}(\mathbf{r})$ is a pure radial function of the distance and is evaluated in reciprocal space to account for the long-range components of the embedding ions, i.e.,

$$v_{loc}(\mathbf{r})=\sum_j\hat{v}_{loc}(\mathbf{r}-\mathbf{R}_j)=\sum_j\sum_{\mathbf{G}\neq 0}\tilde{v}_{loc}(\mathbf{G})e^{-i\mathbf{G}\cdot(\mathbf{r}-\mathbf{R}_j)}$$
$$=\frac{1}{V}\sum_{\mathbf{G}\neq 0}S(\mathbf{G})\tilde{v}_{loc}(\mathbf{G})e^{-i\mathbf{G}\cdot\mathbf{r}}, \quad (38)$$

where $\mathbf{G}$ runs over the reciprocal lattice vectors up to the plane-wave cutoff and $S(\mathbf{G})$ is the structure factor. The short-range second term in Eq. (37) is calculated by evaluating three-center integrals of the form $\langle\phi_\mu^I(\mathbf{r})|v_{nonloc}(\mathbf{r})|\phi_\nu^I(\mathbf{r})\rangle$ in real space[71] where $\{\phi_\mu^I(\mathbf{r})\}$ are the atom-centered basis functions of Region I. This term falls off exponentially and is negligible beyond a few neighboring ions. For consistency, the same type of pseudopotentials were utilized in the *ab initio* and DFT parts of the calculation. The radial parts of the pseudopotentials used in the plane-wave DFT calculation of $\rho_{tot}(\mathbf{r})$ were fitted to well separated spherical Gaussian functions using a Levenberg-Marquardt nonlinear least-squares optimization,[72] to ensure compatibility with the Gaussian orbital-based program we modified for the purpose of the embedding.

We note that since the ionic summation in Eqs. (37) and (38) runs purely over the ions in the surroundings, this results in an implicit ''notched'' environment where atoms in the embedded region are missing in the main cell (as they should be) and in all the neighboring cells (an artifact) due to the periodicity. It is therefore important to construct large enough supercells so that the notches from different cells do not interact via the long-range terms treated in reciprocal space. This is consistent with the calculation of the Hartree term (see below), so that charge neutrality is maintained. At some point it may be possible to reduce the cost of this calculation by using an approximate background density constructed using smaller supercells by exploiting the fact that the density far away from the adsorbate should be unperturbed.

3. Exchange-correlation contribution $-\delta E_{xc}^{int}/\delta\rho_I$

The exchange-correlation contribution to the embedding potential was treated at the LDA or GGA level, consistent with the functional used in the calculation of $\rho_{tot}(\mathbf{r})$. Since this term is short ranged, it was conveniently evaluated on a uniform grid in real space.

4. Hartree contribution $-\delta J^{int}/\delta\rho_I$

The electron-electron repulsion is a long-ranged term and must be handled with care. It can be evaluated in real or reciprocal space. Since the Coulomb potential falls off very slowly with distance, a large number of cells needs to be included for convergence. This is especially so if Region II is effectively infinite, e.g., as in a crystalline bulk or surface. However, in reciprocal space, the long-range component, $\mathbf{G}=0$, can be easily isolated explicitly and dealt with separately.[73] In Fourier space, Eq. (14) becomes

$$\frac{\delta J^{int}}{\delta\rho_I(\mathbf{r})}=\frac{4\pi}{V}\sum_{\mathbf{G}\neq 0}\frac{e^{-i\mathbf{G}\cdot\mathbf{r}}}{G^2}[\tilde{\rho}_{tot}(\mathbf{G})-\tilde{\rho}_I(\mathbf{G})]. \tag{39}$$

D. Calculation of the energies

E_{tot}^{emb} was calculated in the following manner: E_I^{ab} was calculated self-consistently in the presence of $v_{emb}(\mathbf{r})$ and the converged Region I density was then used to evaluate the E_I^{DFT} in the presence of $v_{emb}(\mathbf{r})$. The difference $(E_I^{ab}-E_I^{DFT})$ was substituted in Eq. (16) to correct E_{tot}^{DFT}. A closer analysis of the correction term reveals that the correction arises from the different kinetic-energy and exchange-correlation descriptions in the *ab initio* and DFT calculations, respectively. The other terms exactly cancel out between the two.

IV. APPLICATIONS

A. Li_2Mg_2: Linear and *T* geometries

The embedding scheme was first tested on the same toy model (Li_2Mg_2) used by Abarenkov *et al.*[45] This model was chosen because it is small enough to allow near full CI (nFCI) calculations to be performed for comparison. Both linear and *T* geometries were considered with $R_{Li_2}=3.465$ Å and $R_{Mg_2}=2.543$ Å (Fig. 5, where the shading is consistent with Fig. 1). Two configurations, an infinite and a representative nearby separation, were chosen to examine energy differences.

Regions I and II were first identified. Li_2 and the Mg atom closest to it comprised Region I and the remaining Mg atom comprised Region II. This is a meaningful partition, as one can think of Li_2Mg as the embedded cluster (chemisorption region), and the lone Mg atom as the embedding region (surface). This identification was maintained for both the geometries.

The reference density $\rho_{tot}(\mathbf{r})$ was calculated using a plane-wave cutoff of 300 eV and a large supercell of dimensions 10 Å×10 Å×30 Å. This simulation cell was large enough to prevent any interactions with atoms in neighboring cells. Both LDA[10] and GGA[14] densities were calculated. The Gaussian density $\rho_I(\mathbf{r})$ was updated self-consistently at the spin-restricted HF (RHF) level in the presence of $v_{emb}(\mathbf{r})$. For both Li and Mg, standard contracted Gaussian bases (CGTO) $(4s,4p)/[2s,2p]$[74] were used. The full Mg basis set was placed on the embedding Mg, to minimize the basis set superposition errors (BSSE)[75] and to produce the correct tails of $\rho_I(\mathbf{r})$ around the embedding Mg.[29]

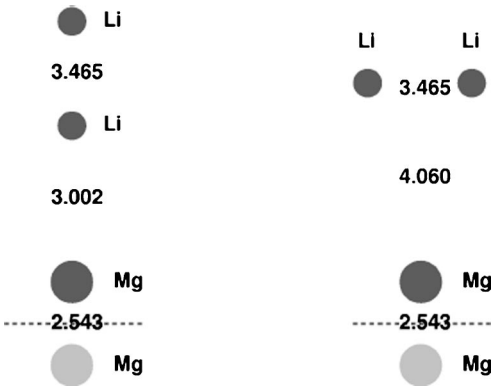

FIG. 5. Linear and T geometries. The linear geometry is shown on the left and T geometry on the right. All distances are in Å. The figures also show the embedded and embedding regions shaded in a manner consistent with Fig. 1.

Two different T_s functionals and their potentials were tested for the embedding potential, the TF−(1/9)vW model[46]

$$T_s^{TF-(1/9)vW}[\rho]=T_{TF}+\tfrac{1}{9}T_{vW}, \tag{40}$$

$$\frac{\delta T_s^{TF-(1/9)vW}}{\delta\rho(\mathbf{r})}=\frac{(3\pi^2)^{2/3}}{2}\rho(\mathbf{r})^{2/3}-\frac{1}{36}\frac{\nabla^2\rho(\mathbf{r})}{\rho(\mathbf{r})}+\frac{1}{72}\frac{|\nabla\rho(\mathbf{r})|^2}{\rho(\mathbf{r})^2} \tag{41}$$

and the Zhao-Levy-Parr (ZLP) model[76]

$$T_s^{ZLP}[\rho]=2^{2/3}c_1\left\langle \rho(\mathbf{r})^{5/3}\left[1-c_2\rho(\mathbf{r})^{1/3}\times\ln\left(1+\frac{1}{c_2\rho(\mathbf{r})^{1/3}}\right)\right]\right\rangle, \tag{42}$$

$$\frac{\delta T_s^{ZLP}}{\delta\rho(\mathbf{r})}=2^{2/3}\frac{5c_1}{3}\rho(\mathbf{r})^{2/3}-2^{5/3}c_1c_2\rho(\mathbf{r})\times\ln\left(1+\frac{1}{c_2\rho(\mathbf{r})^{1/3}}\right)+\frac{2^{2/3}}{3}c_1\rho(\mathbf{r})^{2/3}\left(1+\frac{1}{c_2\rho(\mathbf{r})^{1/3}}\right)^{-1} \tag{43}$$

with $c_1=3.2372$, and $c_2=0.00196$. These two KEDFs were chosen because they have been used successfully in a number of other calculations,[20,22,46] and their potentials have the proper limiting behavior and no divergences.[59] These terms were calculated in real space. The embedding correction to E_{tot}^{DFT} was calculated according to the prescription given in Eqs. (15) and (16). Table I summarizes the results. One should note that the MPn calculations are post-SCF perturbative corrections to the RHF result using ρ_I^{RHF}.

TABLE I. Li_2Mg_2 -linear geometry.

Pure DFT		ΔE (eV)
LDA cluster		−0.5501
GGA cluster		−0.5264
Finite cluster		ΔE (eV)
RHF		−0.1121
MP2		−0.1815
MP3		−0.1755
MP4		−0.1729
nFCI[a]		−0.1565
Embedded cluster[b]	$\Delta E^{TF1/9vW}$ (eV)	ΔE^{ZLP} (eV)
RHF/LDA	−0.3052	−0.4016
MP2/LDA	−0.2027	−0.2881
MP3/LDA	−0.1654	−0.2592
MP4/LDA	−0.1501	−0.2403
RHF/GGA	−0.2816	−0.3779
MP2/GGA	−0.1790	−0.2644
MP3/GGA	−0.1517	−0.2355
MP4/GGA	−0.1378	−0.2166

[a]The near-full CI result for the linear Li_2Mg_2.
[b]Quantum chemistry method for Region I listed first, DFT method for Region II listed second.

A review of the linear-geometry results shows that both LDA and GGA DFT cluster calculations result in an overbinding of a factor of more than 3 compared with nFCI.[77–79] The embedding results presented in the bottom half of the table demonstrate how the embedding helps decrease the overbinding systematically as one improves the level of theory. However, there are noticeable differences in the actual corrections for the two KEDF models. These differences can be attributed to inaccuracies in the KEDF and/or the exchange-correlation models. Nevertheless, the corrections have the same sign for both cases, which is encouraging, and the final energy differences are in good agreement with the nFCI numbers. Calculations were also performed on the T geometry, with the best embedding results yielding 0.1590 eV compared with −0.2983 and −0.2415 eV for the LDA and the GGA, respectively. Even though the embedding result is in error by ~0.15 eV compared with the nFCI result (0.0117 eV), it is still an improvement over the DFT predictions. We shall see that this level of accuracy is reproduced in our next, much more complex, test case.

B. CO/Cu(111)

The method was next applied to study the well characterized CO/Cu(111) system, where the experimental adsorbate binding energy and adsorption site are known for both low and high coverages. Since our embedding scheme is ideally suited to examine a low coverage scenario, we set up our calculation to study a CO coverage of $\Theta_{CO}=0.125$ ML, or 1 CO per eight surface Cu atoms. Infrared and isosteric heat of adsorption data[80] yield a top site for CO and a binding energy of about 0.52 eV at this coverage.

A DFT geometry optimization calculation on the entire system was first performed both at the LDA and the GGA levels. This optimized geometry was then kept fixed throughout the embedding procedure. We emphasize that the current embedding procedure is a single-point calculation for a specific geometry. The supercell used was a (111) slab containing 32 Cu atoms (eight atoms per layer) and a CO placed at a top site on one side of the slab (Fig. 6, where the shading is consistent with Fig. 1). The simulation cell was large enough (5.06 Å×8.76 Å×22.00 Å) so that the interactions between the periodic slab images were negligible.[81–83] The system was partitioned into the chemisorption region (Region I), comprised of one surface Cu atom, three second layer Cu atoms and the CO, and the background (Region II), comprised of the remaining Cu atoms.

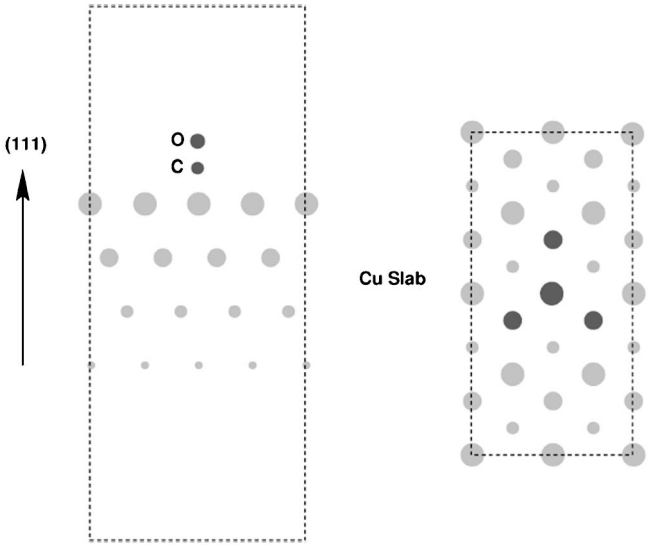

FIG. 6. CO/Cu(111). Figures show the side and top views of the simulation cell with the embedded and embedding regions shaded in a manner consistent with Fig. 1. The optimum bond lengths are $R_{CO}=1.15$ Å, $R_{CCu}=1.86$ Å, and $R_{CuCu}=2.54$ Å, respectively. The different atom sizes indicate the different layers in the slab. Atoms in the topmost layer are represented by the largest circles and so on. Note: image equivalents of the atoms in the unit cell are also represented. The embedded cluster is composed of the CO adsorbate along with one Cu atom from the top layer and three Cu atoms from the second layer of the slab.

The $\rho_{tot}(\mathbf{r})$ was calculated using a large plane-wave cutoff of 850 eV with integrations over the surface Brillouin zone (BZ) performed on a discrete mesh of eight $\mathbf{k}$ points symmetrized over the irreducible BZ. A Gaussian broadening[84] of 0.25 eV was also used to help the convergence. The Gaussian density $\rho_I(\mathbf{r})$ was optimized in the presence of $v_{emb}(\mathbf{r})$ using contracted Gaussian-type orbitals (CGTO) bases $(9s,5p,1d)/[3s,2p,1d]$[85] for C and O, and $(5s,5p,5d)/[3s,3p,2d]$[86] for Cu, and corresponding pseudopotentials.[52] Optimized minimum basis set (MBS) $4s$ functions[87] were placed on the 12 Cu atoms nearest to the cluster to minimize the BSSE and to allow for correct cusps at those nuclei. The $4s$ functions were obtained by performing an atomic HF calculation on Cu using the uncontracted GTO $(5s,5p,5d)$ basis, and the MBS coefficients were taken as the HF $4s$ orbital coefficients without the d contribution.

Since the two subsystems involved are very different in the response sense, a hybrid KEDF model was designed to calculate the relevant contributions to the embedding poten-

TABLE II. CO/Cu(111) binding energies.

Pure DFT	ΔE (eV)
LDA cluster	−1.2138
GGA cluster	−1.1834
LDA slab	−0.8406
GGA slab	−0.7682
Expt[a]	−0.52
Finite cluster	**ΔE (eV)**
RHF	−0.4288
MP2	−1.5973
MP3	−0.9720
MP4	−2.1585
Embedded cluster[b]	**ΔE (eV)**
RHF/LDA	−0.7895
MP2/LDA	−0.7102
MP3/LDA	−0.6824
MP4/LDA	−0.6639
RHF/GGA	−0.7271
MP2/GGA	−0.7030
MP3/GGA	−0.6891
MP4/GGA	−0.6823

[a]The experimental value for CO/Cu(111) for low coverages, $\Theta_{CO}<0.25$.
[b]Quantum chemistry method for Region I listed first, DFT method for Region II listed second.

tial. The extended background was treated using the Wang-Teter-Perrot[62,63] functional

$$T_s^{5/6}[\rho_{\rm tot}]=T_{\rm TF}[\rho_{\rm tot}]+T_{\rm vW}[\rho_{\rm tot}]+T_X^{5/6}[\rho_{\rm tot}], \tag{44}$$

$$\frac{\delta T_s^{5/6}[\rho_{\rm tot}]}{\delta\rho_{\rm tot}(\mathbf{r})}=\frac{\delta T_{\rm TF}[\rho_{\rm tot}]}{\delta\rho_{\rm tot}(\mathbf{r})}+\frac{\delta T_{\rm vW}[\rho_{\rm tot}]}{\delta\rho_{\rm tot}(\mathbf{r})}+\frac{5}{3}\rho_{\rm tot}(\mathbf{r})^{-1/6}\times\int\rho_{\rm tot}(\mathbf{r}')^{5/6}K_{5/6}(\mathbf{r}-\mathbf{r}')d\boldsymbol{\tau}', \tag{45}$$

which was calculated partly in real space ($T_{\rm TF}, T_{\rm vW}$) and partly in reciprocal space ($T_X^{5/6}$). This functional is a reasonable choice as it has the correct LR by construction and yields a good potential as judged by the surface electron density (Fig. 4). The cluster + CO system was treated using the ZLP functional, Eqs. (42) and (43), and was evaluated in real space.

The results presented in Table II show that both DFT/LDA and GGA cluster calculations overestimate the binding energy by about 0.60 eV compared with experiment (0.52 eV). Notice that the numbers are greatly improved at both the LDA/GGA levels when the periodic slab model is used, demonstrating the importance of the correct infinite boundary conditions absent in cluster models. The situation is even worse in the case of the pure finite cluster quantum chemical calculations where one sees spurious oscillations[88] in the binding energies as the level of theory is increased. This can be attributed to the fact that the perturbation series is nowhere near convergent, as well as to the finite size of the cluster. Similar observations of oscillations in adsorbate-finite cluster binding energies with MPn theory have been reported by Bauschlicher.[88] He also found that the series only became convergent for large clusters.

The embedding results in the bottom half of the table are very encouraging, in that the oscillations are quenched out even in a small embedded cluster suggesting that the embedded cluster has some of the same electronic structure characteristics as very large finite clusters. Furthermore, our embedding scheme improves DFT slab results. We point out that a comparative study using various T_S functional models was not performed in this case owing to the expense involved in performing this calculation.

V. DISCUSSION AND CONCLUSION

We have presented and implemented a new embedded cluster method, combining explicit *ab initio* correlation and DFT, which offers the means to systematically improve the description of energetics in a local region. The scheme may be viewed as an extension of a pure DFT-in-DFT embedding formulation,[20] but our scheme offers an improvement via an explicitly correlated *ab initio* calculation of Region I. The procedure involves the usual partitioning of the total system but utilizes no arbitrary orbital localization for the total space or the subspaces, making it quite different from the related approach of Abarenkov *et al.*[45] The scheme is exact in theory, but not in practice, with the main source of ambiguity stemming from the arbitrary nature of the density-functional (both kinetic and exchange-correlation) contribution to $v_{\rm emb}(\mathbf{r})$. Nevertheless, the results from the two applications presented lend support to the procedure and certainly suggest a better understanding of the compatibility of KEDFs and exchange-correlation functionals is needed. Surely the development of better KEDFs should help improve the accuracy of the scheme as well. An improvement that is currently being implemented involves eliminating the dependency of $E_{\rm I}^{\rm DFT}$ on $T_s[\rho_{\rm I}]$. This involves solving the Kohn-Sham equations (at least once) to obtain a set of orbitals that yield the same converged $\rho_{\rm I}$.

Concerning the topic of orbital localization routinely used in embedding schemes, the best route is surely via an optimal Wannier-like unitary localization transformation[60] over occupied orbitals prior to the construction of the embedding operators. This is certainly possible for systems with a band gap, such as insulators, semiconductors, small atomic and molecular clusters, etc., whose density matrices fall off exponentially

$$\lim_{|\mathbf{r}-\mathbf{r}'|\to\infty} P(\mathbf{r},\mathbf{r}')\propto e^{-\beta|\mathbf{r}-\mathbf{r}'|}, \tag{46}$$

where β is proportional to the magnitude of the band gap. In other words, the density matrices in these systems are ''near sighted''[89] or diagonal dominant. Metallic or zero-band-gap systems, on the other hand, pose a different problem, as their density matrices only fall off algebraically[90]

$$\lim_{|\mathbf{r}-\mathbf{r}'|\to\infty} P(\mathbf{r},\mathbf{r}')\propto|\mathbf{r}-\mathbf{r}'|^{-3}, \tag{47}$$

thus not guaranteeing an exponential localization, as in the finite band-gap systems. Even though it has been shown recently[91–93] that metallic density matrices can have better than algebraic falloffs at nonzero temperatures, the problem of fractionally occupied orbitals still stymies the design of a Wannier-like localization transformation, which requires the presence of distinct occupied and unoccupied orbital spaces. It is possible to devise strategies that circumvent this problem by performing subspace localizations on a predetermined or a dynamically partitioned orbital space of the full system.[29,30,34–36,45] Unfortunately, these transformations are not unique and introduce transformation-dependent terms into the theory. In a nutshell, once a system is decomposed into subsystems, there is no single unitary localization transformation that simultaneously leaves all the physical observables of the total system and subsystems unchanged. We refer the interested reader to recent papers by Gutdeutsch *et al.*[34] for an illustrative discussion of these issues.

Further, even if it is theoretically possible to exponentially localize metallic states, there are practical difficulties associated with the problem of orbital localization. For example, a good description of a metal requires a very high quality BZ or **k**-point sampling,[94] requiring the storage of the orbitals over all space at each of these **k** points. The localization calculation can quickly become numerically intractable as a result.[95]

Taking into account the various theoretical and practical issues, we assert that the embedding formulation presented here is not only a practical but also a rather accurate compromise. Since the scheme requires the knowledge of a well-converged reference density ($\rho_{\mathrm{tot}}(\mathbf{r})$) and reference energy ($E_{\mathrm{tot}}$) for the full system (for each geometry) the procedure can become quite expensive for systems which require large supercells. Work to reduce the expense of the technique is in progress. The theory as it stands can be readily extended to open-shell systems, as well as to other procedures like multireference calculations and others. Such extensions are under way. The possibility of generalizing the theory to treat local excited states also exists.

ACKNOWLEDGMENTS

We thank A. Christensen, E. Fattal, and S. Watson for helpful discussions. Financial support for this project was provided by the National Science Foundation, the Air Force Office of Scientific Research and the Army Research Office.

[1] Recent examples include: C. W. Bauschlicher, Jr., J. Chem. Phys. **101**, 3250 (1994); L. Triguero, U. Wahlgren, P. Boussard, and P. Siegbahn, Chem. Phys. Lett. **237**, 550 (1995); P. S. Bagus and G. Paccioni, J. Chem. Phys. **102**, 879 (1995); F. Illas, J. Rubio, J. M. Ricart, and G. Paccioni, *ibid.* **105**, 7192 (1996); A. Clotet and G. Paccioni, Surf. Sci. **346**, 91 (1996); F. Illas, S. Zurita, A. M. Marquez, and J. Rubio, *ibid.* **376**, 279 (1997).

[2] H. Nakatsuji, Prog. Surf. Sci. **54**, 1 (1997).

[3] N. Rösch, P. Sandl, A. Gorling, and P. Knappe, Int. J. Quantum Chem., Symp. **22**, 275 (1988).

[4] E. Wimmer, H. Krakauer, M. Weinert, and A. J. Freeman, Phys. Rev. B **24**, 864 (1981); M. Weinert, E. Wimmer, and A. J. Freeman, *ibid.* **26**, 4571 (1982); H. J. F. Jansen and A. J. Freeman, *ibid.* **30**, 561 (1984); C. L. Fu and A. J. Freeman, *ibid.* **40**, 5359 (1989); W. Mannstadt and A. J. Freeman, *ibid.* **55**, 13 298 (1997); E. Wimmer, C. L. Fu, and A. J. Freeman, Phys. Rev. Lett. **55**, 2618 (1985).

[5] K. Gundersen, K. W. Jacobsen, J. K. Norskov, and B. Hammer, Surf. Sci. **304**, 131 (1994); B. Hammer, M. Scheffler, K. W. Jacobsen, and J. K. Norskov, Phys. Rev. Lett. **73**, 1400 (1994); B. Hammer and J. K. Norskov, *ibid.* **79**, 4441 (1997); J. J. Mortensen, B. Hammer, J. K. Norskov, *ibid.* **80**, 4333 (1998).

[6] C. Stampfl and M. Scheffler, Phys. Rev. B **54**, 2868 (1996); C. M. Wei, A. Gross, and M. Scheffler, *ibid.* **57**, 15572 (1998); C. Stampfl and M. Scheffler, Phys. Rev. Lett. **78**, 1500 (1997); D. Tomanek, S. Wilke, and M. Scheffler, *ibid.* **79**, 1329 (1997); C. Stampfl and M. Scheffler, J. Vac. Sci. Technol. A **15**, 1635 (1997).

[7] P. Hu, D. A. King, M.-H. Lee, and M. C. Payne, Chem. Phys. Lett. **246**, 73 (1995); Q. Ge and D. A. King, *ibid.* **285**, 15 (1998); P. Hu, D. A. King, S. Crampin, M.-H. Lee, and M. C. Payne, J. Chem. Phys. **107**, 8103 (1997).

[8] J. A. White, D. M. Bird, M. C. Payne, and I. Stich, Phys. Rev. Lett. **73**, 1404 (1994); P. A. Gravil, D. M. Bird, and J. A. White, *ibid.* **77**, 3933 (1996); J. A. White, D. M. Bird, and M. C. Payne, Phys. Rev. B **53**, 1667 (1996).

[9] G. te Velde and E. J. Baerends, Chem. Phys. **177**, 299 (1993); P. H. T. Philipsen, G. te Velde, and E. J. Baerends, Chem. Phys. Lett. **226**, 583 (1994); G. Wiesenekker, G. J. Kroes, and E. J. Baerends, J. Chem. Phys. **104**, 7344 (1996); R. A. Olsen, P. H. T. Philipsen, E. J. Baerends, G. J. Kroes, and O. M. Lovvik, *ibid.* **106**, 9286 (1997); P. H. T. Philipsen, E. van Lenthe, J. G. Snijders, and E. J. Baerends, Phys. Rev. B **56**, 13556 (1997).

[10] J. P. Perdew and A. Zunger, Phys. Rev. B **23**, 5048 (1981).

[11] P. Fulde, *Electron Correlations in Molecules and Solids* (Springer, Berlin, 1995), and references therein.

[12] J. P. Perdew, Phys. Rev. B **33**, 8822 (1986); J. P. Perdew, *ibid.* **34**, 7406(E) (1986).

[13] A. D. Becke, Phys. Rev. A **38**, 3098 (1988).

[14] J. P. Perdew and Y. Wang, Phys. Rev. B **43**, 13244 (1992); J. P. Perdew, J. A. Chevary, S. H. Vosko, K. A. Jackson, M. R. Pederson, D. J. Singh, and C. Fiolhais, *ibid.* **46**, 6671 (1992).

[15] J. P. Perdew, K. Burke, and M. Enrzerhof, Phys. Rev. Lett. **77**, 3865 (1997).

[16] One should remember that these exchange-correlation density functionals are purely functions of the local density (LDA) and derivatives (GGA) at a grid point.

[17] Y. M. Juan and E. Kaxiras, Phys. Rev. B **48**, 14944 (1993); A. Garcia, C. Elsässer, J. Zhu, S. G. Louie, and M. L. Cohen, *ibid.* **46**, 9829 (1992); P. Nachtigall, K. D. Jordan, A. Smith, and H. Jónsson, J. Chem. Phys. **104**, 148 (1996); B. Hammer, M. Scheffler, K. W. Jacobsen, and J. K. Norskov, Phys. Rev. Lett. **73**, 1400 (1994); K. Gundersen, K. W. Jacobsen, J. K. Norskov, and B. Hammer, Surf. Sci. **304**, 131 (1994); G. Wiesenekker, G. J. Kroes, and E. J. Baerends, J. Chem. Phys. **104**, 7344 (1996); P. H. T. Philipsen, G. te Velde, and E. J. Baerends, Chem. Phys. Lett. **226**, 583 (1994); B. Hammer, L. B. Hansen. and J. K. Norskov, preprint (1998).

[18] See, for example, J. P. Perdew, K. Burke, and M Ernzerhof, Phys. Rev. Lett. **77**, 3865 (1996); E.I. Proynov, S. Sirois, and D. R. Salahub, Int. J. Quantum Chem. **64**, 427 (1997); D. J. Tozer, N. C. Handy, and W. H. Green, Chem. Phys. Lett. **273**, 183 (1997); M. Filatov and W. Thiel, Mol. Phys. **91**, 847 (1997); T. Van Voorhis and G. E. Scuseria, J. Chem. Phys. **109**, 400 (1998); Y. Zhang and W. Yang, Phys. Rev. Lett. **80**, 890 (1998); D. J. Tozer and N. C. Handy, J. Chem. Phys. **108**, 2545 (1998).

[19] D. E. Ellis, G. A. Benesh, and E. Byrom, Phys. Rev. B **16**, 3308 (1977); **20**, 1198 (1979); H. Zheng, *ibid.* **48**, 14868 (1993); D. E. Ellis, G. A. Benesh, and E. Byrom, J. Appl. Phys. **49**, 1543 (1978); D. E. Ellis, J. Guo, and H. P. Cheng, J. Phys. Chem. **92**, 3024 (1988).

[20] P. Cortona, Phys. Rev. B **44**, 8454 (1991); **46**, 2008 (1992); P. Cortona and A. V. Monteleone, Int. J. Quantum Chem. **52**, 987 (1994).

[21] M. J. Field, P. A. Bash, and M. Karplus, J. Comput. Chem. **16**, 700 (1990); R. D. J. Froese and K. Morokuma, Chem. Phys. Lett. **263**, 393 (1996); T. Matsubara, S. Sieber, and K. Morokuma, Int. J. Quantum Chem. **60**, 1101 (1996); M. Svensson, S. Humbel, and K. Morukuma, J. Chem. Phys. **105**, 3654 (1996); S. Humbel, S. Seiber, and K. Morukuma, *ibid.* **105**, 1959 (1996); F. Maseras and K. Morukuma, J. Comput. Chem. **16**, 1170 (1995).

[22] T. A. Wesolowski and A. Warshel, J. Phys. Chem. **97**, 8050 (1993); **98**, 5183 (1994); T. A. Wesolowski and J. Weber, Chem. Phys. Lett. **248**, 71 (1996).

[23] E. V. Stefanovich and T. N. Truong, J. Chem. Phys. **104**, 2946 (1996); **106**, 7700 (1997).

[24] E. A. Colbourn, Surf. Sci. Rep. **15**, 281 (1992).

[25] J. A. Meijas and J. F. Sanz, J. Chem. Phys. **102**, 327 (1995); J. A. Meijas and J. F. Sanz, Chem. Phys. **191**, 133 (1995).
[26] J. H. Harding, A. H. Harker, P. B. Keegstra, R. Pandey, J. M. Vail, and C. Woodward, Physica B & C **131**, 151 (1985); A. B. Kunz and J. M. Vail, Phys. Rev. B **38**, 1058 (1988); A. B. Kunz, J. Meng, and J. M. Vail, *ibid.* **38**, 1064 (1988).
[27] T. Fox, N. Rösch, and R. J. Zauhar, J. Comput. Chem. **14**, 253 (1993).
[28] T. N. Truong and E. V. Stefanovich, Chem. Phys. Lett. **240**, 253 (1995); T. N. Truong and E. V. Stefanovich, J. Phys. Chem. **99**, 14700 (1995); E. V. Stefanovich and T. N. Truong, Chem. Phys. Lett. **244**, 65 (1995); E. V. Stefanovich and T. N. Truong, J. Chem. Phys. **105**, 2961 (1996); T. N. Truong, U. N. Nguyen, and E. V. Stefanovich, *ibid.* **107**, 1881 (1997).
[29] J. L. Whitten and T. A. Pakkanen, Phys. Rev. B **21**, 4357 (1980); J. L. Whitten, *ibid.* **24**, 1810 (1981); P. Cremaschi and J. L. Whitten, Surf. Sci. **149**, 273 (1985); P. Cremaschi and J. L. Whitten, Theor. Chim. Acta **72**, 485 (1987); P. Madhavan and J. L. Whitten, J. Chem. Phys. **77**, 2673 (1982); J. L. Whitten, in *Cluster Models for Surface and Bulk Phenomena*, edited by G. Pacchioni, P. S. Bagus, and F. Parmigiani, NATO ASI Series B: Physics Vol. 283 (Plenum, New York, 1992), p.375; J. L. Whitten, J. Chem. Phys. **177**, 387 (1993); J. L. Whitten and H. Yang, Int. J. Quantum Chem., Symp. **29**, 41 (1995); J. L. Whitten and H. Yang, Surf. Sci. Rep. **24**, 59 (1996).
[30] J. D. Head and S. J. Silva, J. Chem. Phys. **104**, 3244 (1996).
[31] W. Ravenek and F. M. M. Guerts, J. Chem. Phys. **84**, 1613 (1986).
[32] H. A. Duarte and D. R. Salahub, J. Chem. Phys. **108**, 743 (1998).
[33] H. Sellers, Chem. Phys. Lett. **178**, 351 (1991).
[34] U. Gutdeutsch, U. Birkenheuer, S. Krüger, and N. Rösch, J. Chem. Phys. **106**, 6020 (1997); U. Gutdeutsch, U. Birkenheuer, and N. Rösch, *ibid.* **109**, 2056 (1998).
[35] T. L. Gilbert, in *Molecular Orbitals in Chemistry, Physics, and Biology*, edited by P.-O. Löwdin and B. Pullman (Academic, New York, 1964).
[36] W. H. Adams, J. Chem. Phys. **34**, 89 (1961); **37**, 2009 (1962).
[37] C. Pisani, Phys. Rev. B **17**, 3143 (1978); C. Pisani, R. Dovesi, and P. Carosso, *ibid.* **20**, 5345 (1979); S. Cassasa and C. Pisani, *ibid.* **51**, 7805 (1995); C. Pisani, R. Dovesi, R. Nada, and l. N. Kantorovich, J. Chem. Phys. **92**, 7448 (1990); C. Pisani, J. Mol. Catal. **82**, 229 (1993).
[38] S. Krüger and N. Rösch, J. Phys.: Condens. Matter **6**, 8149 (1994); S. Krüger, U. Birkenheuer, and N. Rösch, J. Electron Spectrosc. Relat. Phenom. **69**, 31 (1994).
[39] J. E. Inglesfield, J. Phys. C **14**, 3795 (1981); G. A. Benesh and J. E. Inglesfield, *ibid.* **17**, 1595 (1984); J. E. Inglesfield and G. A. Benesh, Phys. Rev. B **37**, 6682 (1988); G. A. Benesh and l. S. G. Liyanage, *ibid.* **49**, 17 264 (1994); M.I. Trioni, G. P. Brivio, S. Crampin, and J. E. Inglesfield, *ibid.* **53**, 8052 (1996); G. A. Aers and J. E. Inglesfield, Surf. Sci. **217**, 367 (1989); E. A. Colbourn and J. E. Inglesfield, Phys. Rev. Lett. **66**, 2006 (1991); S. Crampin, J. B. A. N. van Hoof, M. Nekovee, and J. E. Inglesfield, J. Phys.: Condens. Matter **4**, 1475 (1992).
[40] M. Scheffler, C. Droste, A. Fleszar, F. Màca, G. Wachutka, and G. Borzel, Physica B **172**, 143 (1991); G. Wachutka, A. Fleszar, F. Màca, and M. Scheffler, J. Phys.: Condens. Matter **4**, 2831 (1992); J. Bormet, J. Neugebauer, and M. Scheffler, Phys. Rev. B **49**, 17942 (1994); J. Bormet, B. Wenzien, and M. Scheffler, Comput. Phys. Commun. **51**, 381 (1994).
[41] A. R. Williams, P. J. Feibelman, and N. D. Lang, Phys. Rev. B **26**, 5433 (1982); P. J. Feibelman, *ibid.* **35**, 2626 (1989); **49**, 14632 (1994); P. J. Feibelman, Phys. Rev. Lett. **67**, 461 (1991); P. J. Feibelman, Surf. Sci. **313**, L801 (1994).
[42] J. Bernholc, N. O. Lipari, and S. T. Pantelides, Phys. Rev. Lett. **41**, 895 (1978); J. Bernholc, N. O. Lipari, and S. T. Pantelides, Phys. Rev. B **21**, 3545 (1980).
[43] A. Szabo and N. S. Ostlund, *Modern Quantum Chemistry: Introduction to Advanced Electronic Structure Theory* (Dover, New York, 1996); *Methods of Electronic Structure Theory*, edited by Henry F. Schaefer III (Plenum, New York, 1977).
[44] B. Kirtman and C. de Melo, J. Chem. Phys. **75**, 4592 (1981); B. Kirtman, *ibid.* **79**, 835 (1983); B. Kirtman, Int. J. Quantum Chem. **55**, 103 (1995).
[45] I. V. Abarenkov, V.L. Bulatov, R. Godby, V. Heine, M. C. Payne, P. V. Souchko, A. V. Titov, and I. I. Tupitsyn, Phys. Rev. B **56**, 1743 (1997).
[46] See, for example, R. G. Parr and W. Yang, *Density Functional Theory of Atoms and Molecules* (Oxford, New York, 1989); R. M. Dreizler and E. K. U. Gross, *Density Functional Theory* (Springer, Berlin, 1990), and references therein.
[47] M. Levy, Proc. Natl. Acad. Sci. USA **76**, 6062 (1979); M. Levy, Phys. Rev. A **26**, 1200 (1982); M. Levy and J. P. Perdew, in *Density Functional Methods in Physics*, edited by R. M. Dreizler and J. da Providência (Plenum, New York, 1985), p. 11.
[48] W. Kohn and L. J. Sham, Phys. Rev. **140**, 1133 (1965).
[49] M. C. Payne, M. P. Teter, D. C. Allan, T. A. Arias, and J. D. Joannopoulos, Rev. Mod. Phys. **64**, 1045 (1992).
[50] M. Dupuis, A. Marquez, and E. R. Davidson, ''HONDO 95.3 from CHEM-Station,'' IBM Corporation, Neighborhood Road, Kingston, New York (1995).
[51] W. E. Pickett, Comput. Phys. Rep. **9**, 115 (1989).
[52] G. B. Bachelet, D. R. Hamann, and M. Schlüter, Phys. Rev. B **26**, 4199 (1982); N. Troullier and J. L. Martins, *ibid.* **46**, 1754 (1992).
[53] Care must be taken while projecting the Gaussian density ($\rho_I(\mathbf{r})$) onto a grid. The quality of the grid also depends sensitively on the type of atoms present in the calculation. Uniform grids $25\times25\times80$ and $30\times60\times120$ were used to represent the electron densities for the Li_2Mg_2 and CO/Cu(111) systems, respectively.
[54] L. H. Thomas, Proc. Cambridge Philos. Soc. **23**, 542 (1927); E. Fermi, Rend. Accad., Lincei **6**, 602 (1927); E. Fermi, Z. Phys. **48**, 73 (1928).
[55] C. F. von Weizsäcker, Z. Phys. **96**, 431 (1935).
[56] N. Govind, J. Wang, and H. Guo, Phys. Rev. B **50**, 11175 (1994); N. Govind, J. L. Mozos, and H. Guo, *ibid.* **51**, 7101 (1995).
[57] V. Shah, D. Nehete, and D. G. Kanhere, J. Phys.: Condens. Matter **6**, 10773 (1994); V. Shah, D. G. Kanhere, C. Majumder, and D. P. Das, *ibid.* **9**, 2165 (1997); D. Nehete, V. Shah, and D. G. Kanhere, Phys. Rev. B **53**, 2126 (1996).
[58] H. Lee, C. Lee, and R. G. Parr, Phys. Rev. A **44**, 768 (1991).
[59] Y. A. Wang, N. Govind, and E. A. Carter (unpublished).
[60] N. W. Ashcroft and N. D. Mermin, *Solid State Physics* (Holt Rinehart and Winston, New York, 1976).
[61] J. Lindhard, K. Dan. Vidensk. Selsk. Mat. Fys. Medd. **28**, 8 (1954).
[62] L.-W. Wang and M. P. Teter, Phys. Rev. B **45**, 13196 (1992).
[63] F. Perrot, J. Phys.: Condens. Matter **6**, 431 (1994).
[64] M. Pearson, E. Smargiassi, and P. A. Madden, J. Phys.: Condens. Matter **5**, 3321 (1993); M. Foley, E. Smargiassi, and P. A. Madden, *ibid.* **6**, 5231 (1994); E. Smargiassi and P. A. Madden, Phys. Rev. B **49**, 5220 (1994); **51**, 117 (1995).
[65] Y. A. Wang, N. Govind, and E. A. Carter, Phys. Rev. B **58**, 13465 (1998).
[66] For example, D. G. Pettifor, *Bonding and Structure of Molecules and Solids* (Clarendon, Oxford, 1995).
[67] M. Foley and P. A. Madden, Phys. Rev. B **53**, 10589 (1996); **55**, 4941 (1997).
[68] P. Hohenberg and W. Kohn, Phys. Rev. **136**, B864 (1964).
[69] L. Vitos, H. L. Skriver, and J. Kollár, Phys. Rev. B **57**, 12611 (1998).
[70] E. Chacón, J. E. Alvarellos, and P. Tarazona, Phys. Rev. B **32**, 7868 (1985); P. García-González, J. E. Alvarellos, and E. Chacón, *ibid.* **53**, 9509 (1996); **57**, 4857 (1998); P. García-González, J. E. Alvarellos, and E. Chacón, Phys. Rev. A **54**, 1897 (1996); **57**, 4192 (1998).
[71] L. R. Kahn, P. Baybutt, and D. G. Truhlar, J. Chem. Phys. **65**, 3826 (1976).
[72] W. H. Press, S. A. Teukolsky, W. T. Vetterling, and B. P. Flannery, *Numerical Recipes in Fortran* (Cambridge University, New York, 1992).
[73] The $\mathbf{G}=0$ components of the Hartree, ion-electron and ion-ion terms exactly cancel each other. However, in practice a residual constant from the pseudopotential core term may be present after the cancellations, but this just constitutes an overall shift in the total energy.
[74] W. J. Stephens, H. Basch, and M. Krauss, J. Chem. Phys. **81**, 6026 (1984).
[75] S. F. Boys and F. Bernardi, Mol. Phys. **19**, 553 (1970).
[76] Q. Zhao, M. Levy, and R. G. Parr, Phys. Rev. A **47**, 918 (1993); P. Fuentealba and O. Reyes, Chem. Phys. Lett. **31**, 232 (1995).
[77] Full CI calculations were performed on the isolated Li_2 and Mg_2 fragments and a large-scale multi-reference singles and doubles CI calculation (MRSDCI) was performed on the total system using the program MELD (see Ref. 78). The iterative natural orbital approach (see Ref. 79) was utilized for the MRSDCI. The final MRSDCI had a dimension of 380153 for the linear geometry and 297326 for the T geometry, which are about a third of the FCI dimension. The final MRSDCI energies are very close to the FCI values.
[78] *A Many Electron Description*, originally written by L. McMurchie, S. Elbert, S. Langhoff, E. R. Davidson, and further advanced by D. Rawlings and D. Feller, Quantum Chemistry Group, Indiana University, Bloomington, Indiana.
[79] C. F. Bender and E. R. Davidson, J. Phys. Chem. **70**, 2675 (1966); C. F. Bender and E. R. Davidson, J. Chem. Phys. **47**, 4972 (1967).
[80] P. Hollins and J. Pritchard, Surf. Sci. **89**, 486 (1979); R. Raval, S. F.

Parker, M. E. Pemble, P. Hollins, J. Pritchard, and M. A. Chesters, *ibid.* **203**, 353 (1988).
[81] One does not need to create a dipole free unit cell because CO has such a small dipole moment (0.122 D). See Refs. 82 and 83.
[82] J. S. Muenter, J. Mol. Spectrosc. **55**, 490 (1975).
[83] 1 D=1 debye=10^{-18}esu cm=3.33×10^{-30} C m.
[84] M. J. Gillan, J. Phys.: Condens. Matter **1**, 689 (1989).
[85] T. H. Dunning, Jr., and P. J. Hay, in *Methods of Electronic Structure Theory*, edited by H. F. Schaeffer III (Plenum, New York, 1977), Vol. 2.
[86] P. J. Hay and W. R. Wadt, J. Chem. Phys. **82**, 299 (1985).
[87] ζ_s=8.1760, 2.5680, 0.9587, 0.1153, 0.0396 and C_s=0.031 762, −0.074808, 0.132745, −0.505715, −0.580208.
[88] C. W Bauschlicher, Jr., J. Chem. Phys. **101**, 3250 (1994).
[89] W. Kohn, Int. J. Quantum Chem. **56**, 229 (1995).
[90] W. Kohn, Phys. Rev. **115**, 809 (1959); W. Kohn, Phys. Rev. B **7**, 4388 (1973); W. Kohn, in *Condensed Matter Theories*, edited by L. Blum and F. B. Malik (Plenum, New York, 1993), Vol. 8.
[91] R. Baer and M. Head-Gordon, Phys. Rev. Lett. **79**, 3962 (1997).
[92] S. Ismail-Beigi and Tómas Arias, Los Alamos preprint cond-mat/9805147.
[93] S. Goedecker, Los Alamos preprint cond-mat/9806073.
[94] H. J. Monkhorst and J. D. Pack, Phys. Rev. B **13**, 5188 (1976).
[95] In practice, localization can be time consuming even in the case of insulators and semiconductors where an exponential localization is theoretically possible.